

Learning Multiple Sound Source 2D Localization

Guillaume Le Moing^{1,2,†}, Phongtharin Vinayavekhin¹, Tadanobu Inoue¹
Jayakorn Vongkulbhisal¹, Asim Munawar¹, Ryuki Tachibana¹, and Don Joven Agravante¹
Corresponding authors: guillaume.le_moing@mines-paristech.fr, pvmilk@jp.ibm.com

¹IBM Research, Tokyo, Japan

²MINES ParisTech - PSL Research University, Paris, France

Abstract—In this paper, we propose novel deep learning based algorithms for multiple sound source localization. Specifically, we aim to find the 2D Cartesian coordinates of multiple sound sources in an enclosed environment by using multiple microphone arrays. To this end, we use an encoding-decoding architecture and propose two improvements on it to accomplish the task. In addition, we also propose two novel localization representations which increase the accuracy. Lastly, new metrics are developed relying on resolution-based multiple source association which enables us to evaluate and compare different localization approaches. We tested our method on both synthetic and real world data. The results show that our method improves upon the previous baseline approach for this problem.

Index Terms—2D Sound Localization, Multiple Sound Sources, Spatial Audio Analysis, Microphone Arrays, Deep Learning

I. INTRODUCTION

Sound source localization (SSL) is an important topic in audio signal processing. Its output is a pose/location representation which is then used for a variety of different applications such as monitoring of domestic activities, speech enhancement and robotics. The most common approach of SSL is direction of arrival (DOA) estimation [1]–[3]. In DOA, the location is represented as one or more angles of the sound direction. Since the full pose is not represented, it is ambiguous. This ambiguity needs to be resolved before it can be used in several applications. For example, in the monitoring of domestic activity, a good location representation is the 2D point in a floor plan. The DOA output is ambiguous as it points toward a specific angle without depth information. To handle these applications, it is possible to combine the result of multiple DOA setups to produce the necessary 2D position information. A detailed review of such methods is given in [4]. However, not all of these methods are suitable in the case of multiple sound sources. A well-known problem of these methods is the so-called *association ambiguity* [5], [6], whereby these methods produce more candidates than there are actual sources. Although some solutions have been proposed [7], [8], this is still an active research area. Differently from DOA combination methods, this paper is concerned with SSL that directly produces a suitable 2D position representation as an output. Since this is difficult to do directly, in this work we propose and evaluate the use of deep learning methods.

Recently, applying deep neural networks (DNNs) to acoustic applications has gained popularity [1]–[3], [9]–[14]. A data-

driven approach allows to directly learn the complex mapping from sound features to source locations. There are works showing that DNN-based approaches are better than classical methods in the presence of noise and reverberations [1]. However, research on 2D deep acoustic localization is still at an early stage and there are still several open issues. An important related work has shown that it is possible to output the Cartesian point coordinates directly from raw sound [11], or from preprocessed features [12]. However, because the output structure of a DNN needs to be pre-defined, this approach is limited to a fixed number of sound sources which should also be reflected in the training data. The networks in [11], [12] were only designed for a single source hence the approach can not handle multiple sound sources. In [13], multiple sound sources are handled by outputting the coordinates for a predefined number of different sound classes. This tackles multiple source localization because different sound classes can be active simultaneously. However, this approach does not work with simultaneous same-class sound sources. Another method to handle multiple sources configures the network output as a finite set of candidate locations [10]. The output is then trained as a binary classifier whether a source is active or not in that particular location. In [14], a 3D DOA is proposed where they introduce an intermediate output layer, using a *regression-based* approach. However, it still needs a binary classifier to identify active sources. For SSL, these *classification-based* methods appear to be the most common approach for multiple source 2D acoustic localization by deep learning. A clear limitation of this method is in scaling towards finer resolutions as a higher number of output candidates are required. This paper aims to solve these issues.

The main contributions of this paper are: (1) We propose two novel representations of source location for DNN outputs [Section II-B]. The first represents locations as probability distributions (heatmap), while the second represents locations by combining classification-based grid and relative position (refined grid). The results show that both representations increase the accuracy. (2) We propose to use an encoding-decoding network architecture for 2D SSL and provide two improvements: sharing encoders between microphone arrays and pairing features among microphones [Section II-A]. These improvements allow the network to generalize better when there is less training data available. (3) When there are multiple sound sources, it is difficult to evaluate the performance of SSL methods because the association between predicted and

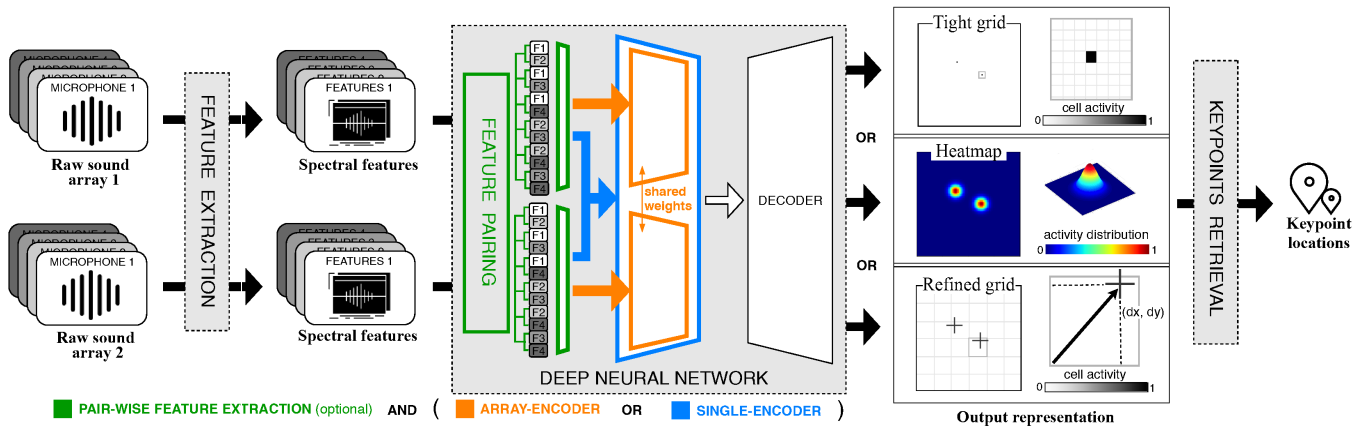


Fig. 1: Outline of the localization framework

ground truth sources can be ambiguous. Inspired by [14], we introduce a novel and comprehensive evaluation metric using resolution-based keypoint association [Section III-B]. (4) Finally, we perform extensive experiments on both synthetic and real world data [Section IV]. We also propose a strategy to improve the training of classification-based methods with a finer resolution grid for a fair comparison [Section II-B]. The results show that the proposed methods outperform the existing methods in all aspects.

II. MULTIPLE SOUND SOURCE 2D LOCALIZATION

The framework for 2D multiple SSL is shown in Fig. 1. The input is raw sound from multiple microphone arrays and the final output is source keypoint locations. The first step is to extract short-time Fourier transform (STFT) features from all the sound channels. Similar to [3], we are using the real and imaginary part of the spectrograms, discarding the zero-frequency component. The STFT features are fed to a neural network which outputs a representation for source locations. The neural network is trained by supervised learning from labeled data. Finally, a post-processing step transforms location representations into 2D keypoint locations. The next subsections detail the major points of our method.

A. Deep Neural Network Architecture

The architecture has two main components. The first component *encodes* spectral features into deep features, while the second component *decodes* them to produce the target location representations. For this *encoder-decoder* configuration, the simplest approach would be to pass the features of all microphones of all arrays at once through the same encoder and then generate location representations by processing the features with a decoder. Here, we propose two improvements for the architecture which are highlighted in Fig. 1.

Array-encoder Instead of feeding all of the features to the same encoder, we propose to have a different encoder for each microphone array. This is similar to classical methods which tackle 2D localization by combining features computed at the array level. The intuition is that the use of multiple encoders helps the model to decompose the localization task into

simpler subtasks. Moreover, when two or more microphone arrays have similar properties and are placed in locations with similar reverberation signatures, the weights of their encoders can be shared because the deep features learned should be similar and independent of the array. This allows the encoders to share their training data, resulting in better generalization with a smaller amount of total training data.

Microphone pair-wise features Most classical methods process microphone signals by pairs to get localization cues. For instance, some methods localize sources by identifying the delay or the difference of attenuation of sound level between pairs of microphones. We reflect this idea in our architecture by treating the input as pairs of microphones rather than a sequence of individual channels. Specifically, the spectral features are duplicated and rearranged so that all combinations of channels in the array can figure side by side. Then, an additional convolutional layer, with kernel and stride of 2, is added before the encoder to extract pair-wise features. This modification can be applied either on the original architecture or on top of the array-encoder modification.

B. Output Representation

The DNN output representations are also illustrated in Fig. 1 and detailed hereafter. We start by explaining a baseline representation, then proceed to the two proposed representations that aim to increase the localization accuracy.

Tight grid (TG-rep) This is the baseline representation. The 2D environment is divided into an $M \times N$ grid. Localization is done at the level of a cell, c , by a binary labeling of its activity, A_c . Active cells, having a sound source inside, are labeled as ($A_c = 1$) so that ($A_c = 0$) for inactive cells. The output is represented by an $M \times N \times 1$ tensor. The loss function is a standard binary cross entropy (BCE) loss done cell-wise:

$$\text{BCE}(A_c^{gt}, A_c^p) = -A_c^{gt} \log(A_c^p) - (1 - A_c^{gt}) \log(1 - A_c^p), \quad (1)$$

where A_c^{gt} is the ground truth label and A_c^p is predicted by the model. Applying (1) naïvely has the problem that precision is directly proportional to the output tensor size. That is, a finer grid with more cells is required for a higher precision. This

leads to a high class imbalance between active and inactive cells. Class imbalance is a common problem in machine learning for classification. To mitigate this, we introduce weights in the loss function to encourage predictions:

$$L_{TG} = \sum_{\text{active } c} \text{BCE}(A_c^{gt}, A_c^p) + \lambda \sum_{\text{inactive } c} \text{BCE}(A_c^{gt}, A_c^p). \quad (2)$$

Heat map (HM-rep) This representation adopts the same grid resolution as that of the TG-rep. But instead of binary labels, locations are represented as probability distributions. Since the output is distributed across a region of cells, the model can gradually learn to predict the target output. Moreover, *sub-cell* accuracy can be obtained since the center of the probability distribution can be anywhere. In our implementation, the location representation is an aggregation of 2D discretized Gaussian distributions centered at the source locations where the aggregation function is the maximum function. A similar representation was adopted in [2] for 1D DOA estimation. In order to facilitate the training, the representation is normalized to $[0, 1]$. The output is represented by an $M \times N \times 1$ tensor, while the loss function between predicted and ground truth heatmap is the mean squared error (MSE). At the cell level, the MSE between ground truth cell activity A_c^{gt} and predicted cell activity A_c^p is:

$$\text{MSE}(A_c^{gt}, A_c^p) = \frac{(A_c^{gt} - A_c^p)^2}{\text{number of cells}}. \quad (3)$$

Therefore, the loss for HM-rep is:

$$L_{HM} = \sum_c \text{MSE}(A_c^{gt}, A_c^p). \quad (4)$$

Refined grid (RG-rep) This novel representation combines the TG-rep approach with direct location regression methods [11], [12]. It is difficult to train TG-rep for finer grids, while direct regression cannot be used with a varying number of sound sources. Combining them allows the network to overcome both limitations. This was inspired by the representation in visual object detection [15]. Similar to TG-rep, the network first predicts the source location at the cell level. Then, the prediction is refined by regressing the relative position $P_c = (dx, dy)$ of the source along x and y axes within the cell. This 2-step approach allows for a coarser grid. The output is represented by an $M \times N \times 3$ tensor where the last dimension combines the probability that a cell is active and its relative position. To learn whether a cell is active, we use BCE together with weight λ_1 to handle the imbalance issue similarly to (2). For the relative position loss, we compute the MSE between predicted P_c^p and ground truth P_c^{gt} relative positions. Similar to [15], the relative position loss is only applied to cells containing an active source. We also introduce a weight for the relative position loss to balance both classification and relative position objectives. Combining these we have:

$$L_{RG} = \sum_{\text{active } c} \text{BCE}(A_c^{gt}, A_c^p) + \lambda_1 \sum_{\text{inactive } c} \text{BCE}(A_c^{gt}, A_c^p) + \lambda_2 \sum_{\text{active } c} \text{MSE}(P_c^{gt}, P_c^p). \quad (5)$$

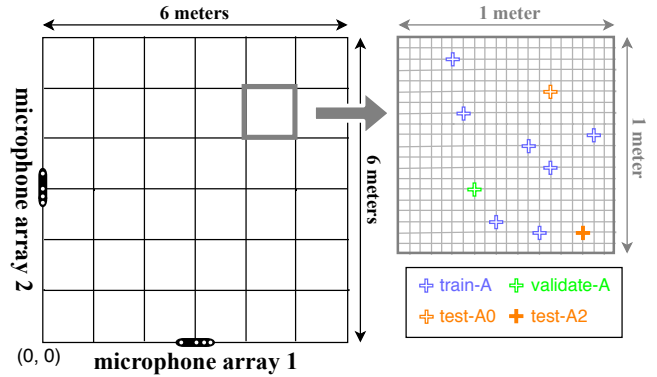


Fig. 2: Environment Layout Configuration

C. Keypoint Retrieval

During inference the network output is converted into sound source 2D coordinates, later referred to as keypoint locations. The method for each representation is described below.

TG-rep We threshold each cell to identify whether there is a sound source inside. Depending on sound activity, the weighted classification loss, (2) can encourage the network to predict the neighboring cells to be active. Simply thresholding the network output can be insufficient. To improve this, Gaussian smoothing and non-maximum suppression (NMS) can be applied.

HM-rep The resulting heatmap is convolved with a Gaussian kernel, with the same standard deviation as the 2D discretized Gaussian used to produce the ground truth. This also filters out high frequency noises. Then, to recover local maxima, NMS is applied such that only the maxima with source probabilities over the threshold are selected as keypoint locations. Finally, a *sub-cell* location is calculated for each keypoint by considering the surrounding cell locations of size 10×10 and then weight-averaging their probabilities.

RG-rep When the source location is near the edge of a cell, the network tends to predict the surrounding cells to be active. NMS is applied to filter these out. As before, only cells with a probability higher than a certain threshold are selected as sources. Taking the predicted relative position of these maxima provides the final keypoints.

III. EXPERIMENTAL SETUP

A. Dataset

We consider as our environment a confined space of 6×6 meters within a large empty office room with a thin carpet floor. Two linear microphone arrays, from a *Kinect Xbox One*¹, with a layout depicted in Fig. 2, are used for recordings. The sound sources are from a large set of classical, funk and jazz songs. From these, 6s excerpts are taken. The classical and funk excerpts are played when recording training, validation and testing data splits. The jazz excerpts are used to capture additional testing data to verify the generalizability of the model. One or more sources at various locations can

¹Microsoft; <http://www.xbox.com/en-US/xbox-one/accessories/kinect>

be active at the same time. When multiple sources are active, we set the minimum distance between sources to be 2 meters. This limitation eases the evaluation process from the need to separate source pairs that are close to each other.

In this paper, we perform experiments in both a simulated and a real world environment with the same layout configuration. Pyroomacoustics [16] is used as the simulated environment. No noise or echo is simulated. We synthesize the dataset by generating 160ms audio samples on a 5x5 cm resolution grid. The sound power of the samples vary widely. To prevent including silent pauses in the dataset, we added thresholding on the average L1-norm of the amplitude.

Capturing and labeling real world audio samples that cover the whole target environment with various source location combinations requires a lot of effort. To ease this process, we take advantage of the fact that sound can be superposed. That is, we only record a single source at a time and later combine audio samples to cover the multiple source cases. To get the real world dataset, we begin by dividing a target environment into 36 cells of 1x1 meter grid. Within each cell, we randomly choose a set of sound source positions in a grid of 5x5 cm resolution, we then play musical excerpts of a specific genre in a random order through the speaker of a mobile phone and capture 10s audio clips. In each cell, we record 7, 1, 1 positions for training, validation and testing data splits, respectively. Audio samples of 160ms are generated by randomly choosing or mixing one or more segments of these audio clips. We perform this for all data splits independently. For instance, the training split has $36 \times 7 = 252$ pieces of 10s audio clips. We randomly choose and mix audio segments to create 10^5 audio samples. We refer to this as a real world dataset with augmentation.

To confirm that our augmentation for multi-source is valid, we also capture samples of the actual case - where multiple sources are present simultaneously in the scene. It takes a lot of effort to capture and label source locations for each data so there are fewer data samples for this case. In particular, we only capture this type of data in a limited number of location sets (labels) but since the sound excerpt (input) is varying, each location provides 10 *different* samples. The process for recording this dataset is similar but with multiple sources playing at the same time. Finally, we also selected generated segments with sufficient energy similar to synthetic set. The details for the datasets are shown in Table I. Datasets with one or two sources contain equal amount of samples for both.

B. Evaluation metrics

Using the corresponding keypoint retrieval method described in Section II-C, we obtain a list of 2D coordinates as source locations. To evaluate this result, the two common distance metrics in the SSL literature are root mean square error (RMSE) [6] and mean average error (MAE) [2]. We choose RMSE so as to penalize when the model makes large prediction errors. RMSE is well suited for single SSL as there is a direct mapping from a predicted keypoint (PK) to a groundtruth keypoint (GK). However, in multiple SSL where

TABLE I: Datasets Used in Experiments

Dataset	Split	Excerpts	# of Srcs	Samples
Synthetic	train-S	classical-funk	1 or 2	100000
	validate-S	classical-funk	1 or 2	5000
	test-S0	classical-funk	1 or 2	5000
	test-S1	classical-funk	3	2500
	test-S2	jazz	1 or 2	5000
Real world with Augmentation	train-A	classical-funk	1 or 2	100000
	validate-A	classical-funk	1 or 2	5000
	test-A0	classical-funk	1 or 2	5000
	test-A1	classical-funk	3	2500
	test-A2	jazz	1 or 2	5000
Real world	test-R0	classical-funk	1 or 2	600
	test-R1	classical-funk	3	300
	test-R2	jazz	1 or 2	600

*youtu.be/ : classical [8f-CFlyNwLE], funk [thUQr7Q1vCY], jazz [oGkkusOMFj0]

the number of source keypoints is unknown beforehand, such a mapping is not straightforward. Previously, Alexandridis *et al.* [17] circumvent the issue by allowing one PK to be associated with more than one GK. However, this method only takes into account the closest PK to every GK and does not reflect mismatch in the number of PKs and GKs.

Instead, we propose to use a resolution-based association method and then use precision, recall, and F1 scores as metrics to account for the varying number of keypoints. To compute these, we first match a PK to a GK if their distance is below the resolution threshold. We then define true positives (TP) as the number of GKs that are matched (note that we count the number of GKs, not the matches); false positives (FP) as number of PKs minus TP; and false negatives (FN) as the number of unmatched GKs. Thus, these metrics penalize all possible mismatches between PKs and GKs. We consider 2 resolution values of 0.3 and 1 meters to account for fine and coarse localization. In addition, since precision, recall, and F1 do not account for distance error, we also include RMSE of the TP as another metric. While we propose to use 4 metrics, we relied for the most part on F1-score and RMSE to discriminate between methods because they give a global understanding of the localization performance whereas precision and recall provide insights to support the interpretation.

C. Experimental Protocols

During experiments, samples consist of two clips of four channel 160ms audio sampled at 16kHz. This is captured with two identical microphone arrays. For each array we extract STFT features with Hamming windows of 32 ms with 50% overlap, resulting in a shape of 8x9x256 (channel \times temporal \times frequency), where the real and imaginary part of the STFT are stacked together in the first axis $[R_1, \dots, R_4, I_1, \dots, I_4]$. The full details are tabulated in Table II.

Experiments are conducted on synthetic datasets and real world datasets separately. The models trained with synthetic data are used on the synthetic test data (test-S). Similarly, the models trained with real world augmented dataset are used to predict on both augmented (test-A) and real world (test-R) datasets. The optimal threshold value for all keypoint retrieval methods are determined empirically to be 0.6, except

TABLE II: Deep neural network detailed architecture

Block	Filters	Kernel	Conv type	Norm	Activation
Input	Spectral features (one array): 8x9x256				
Pair-wise feature extraction	Pairs of microphones (one array): 24x9x256				
	Reshape: 24x9x256 \rightarrow 9x1x24x256				
	8	2x7	conv2d	bn2d	LeakyReLU
Encoder	Reshape: 9x8x12x256 \rightarrow 96x9x256				
	128	1x5	conv2d	bn2d	LeakyReLU
	64	1x3	conv2d		LeakyReLU
	32	1x3	conv2d		LeakyReLU
	16	9x4	conv2d		LeakyReLU
	Reshape: 16x1x32 \rightarrow 512x1x1				
Decoder	256	3x3	dconv2d	bn2d	ReLU
	128	3x3 / 2x2	dconv2d	bn2d	ReLU
	64	3x3	dconv2d	bn2d	ReLU
	32	3x3	dconv2d	bn2d	ReLU
	16	3x3	conv2d		ReLU
	8	3x3	conv2d		ReLU
	1 / 3	3x3	conv2d		ReLU
Output	TG-rep & HM-rep: 1x81x81		RG-rep: 3x6x6		

the improved version of TG-rep which is set to 0.1 due to a smoothing effect from the Gaussian kernel. All models were trained for 200 epochs and the weights that result in the best F1-score on the validation data are used. The ADAM optimizer is used with an initial $lr = 0.0001$, $\beta = (0.5, 0.999)$ and a batch size of 128 samples.

First, we compare output representations by fixing the network architecture. Our experiments have a square environment so $N = M$ for all representations. **TG-rep** is trained using $\lambda = 0.01$ in Eq. (2). To get the keypoint locations, we apply both naïve thresholding (baseline) and the improved version using NMS (improved). Groundtruth heatmaps of **HM-rep** are generated using a Gaussian with $\sigma^2 = 0.1$. This results in $\sim 1m$ of location uncertainty. For HM-rep, we use an output representation with a granularity of 10cm. To cope with the situation where the source is at the edge, the margin is added and results in a grid of $N = 81$. For simplicity, we choose TG-rep to have the same grid size N . For **RG-rep**, the grid number $N = 6$ and $(\lambda_1, \lambda_2) = (0.25, 10)$ in Eq. (5).

Second, we verify the effect of changes on the network architecture while fixing the output representation. Three configurations of the network are compared. **Single-encoder** is a baseline architecture where features of all microphones of all arrays are inputted to the encoder at once. **Array-encoder** represents the architecture that separates the encoder for each array and shares their weights. **Combined** is an architecture that uses both modifications by separating the encoder and rearranging channels by pairs of microphones. At the array-level, input features are duplicated and rearranged into a shape of $24x9x256$; $[(R_1, R_2), (R_1, R_3), \dots, (R_3, R_4), (I_1, I_2), (I_1, I_3), \dots, (I_3, I_4)]$.

IV. EXPERIMENTAL RESULTS

The output representation and architecture design results are given in Table III. Evaluation metrics were computed for resolutions of 0.3 and 1.0 meter for synthetic, augmented real and real test sets.

Output Representation Comparison With a naïve keypoint retrieval approach (only thresholding), TG-rep (baseline)

showed a competitive recall but with a poor precision across all test sets. The weighted loss introduced in Eq. (2) encourages the model to make multiple guesses at the vicinity of each expected source location. Therefore, the number of FP can be high. The proposed keypoint retrieval method greatly enhances the localization performance in TG-rep (improved). Nonetheless, the two introduced output representations (RG-rep and HM-rep) consistently outperform the TG-rep output representation by a large margin. Both introduced output representations have similar performance. However, out of the two, HM-rep seems to better generalize across the various testing settings. For this reason, HM-rep has been chosen for the comparison of architecture designs.

Architecture Design Comparison This comparison is done on two training settings: full training set and limited training set (10%), while all test sets are identical. The results show that our proposed changes to the architecture improve the overall localization performance. The performance gap is relatively small with the full training set; however, with the limited training set, the margin between single-encoder and array-encoder architectures is significant. This suggests that the proposed architecture requires less data to train. The combined architecture does not always outperform the array-encoder architecture. Both methods seem to lead to equivalent overall results most of the time.

Impact of Resolution Looking at the output representation and architecture design results, we can see a rise in both precision and recall from fine resolution (0.3m) to coarser resolution (1m). The reason is that more associations between ground truth and predicted keypoints can be made. As unassociated predicted keypoints result in bad precision (FP is high) and unassociated ground truth keypoints result in bad recall (FN is high), then augmenting the resolution leads to higher precision, recall and F1-score. However, RMSE increases with the resolution because keypoints can be further away.

Generalization on Source Number and Musical Genres Additional localization performance results for one, two, and three sources as well as musical genres can be found in Table IV. Results are given for the best output representation (HM-rep), best performing model (Combined) and resolution of 1 meter because it seems more suitable as pairs of keypoints tend to be around 0.3 meters away on average for tests on real data with a resolution of 1 meter. Even though models were trained with 1 and 2 sources, the results for 3 simultaneous sources are still relatively good compared to the cases where there are 1 and 2 sources. A model trained on synthetic dataset (train-S) has similar performance on *classical-funk* and *jazz* musical genres. But a model trained on real world with augmentation dataset (train-A) does not generalize as much to other musical genres.

Synthetic, Augmented and Real World Data Comparison Despite the significant recording and labeling effort, the models trained on real world data still lack diversity compared to the synthetic environment. This is also reflected by the performance drop from synthetic to real world with augmentation. An additional performance decrease is observed

TABLE III: Output representation and architecture results

Dataset		test-S0								test-A0								test-R0							
Resolution		0.3 m				1 m				0.3 m				1 m				0.3 m				1 m			
Output rep.	DNN arch.	Pre	Rec	F1↑	RMSE↓																				
TG-rep (baseline)	Combined	.38	.87	.53	.15	.40	.92	.56	.23	.29	.34	.31	.20	.55	.65	.59	.44	.12	.24	.16	.19	.29	.56	.38	.50
TG-rep (improved)		.86	.85	.85	.11	.95	.94	.94	.20	.35	.35	.35	.20	.63	.64	.64	.45	.15	.25	.19	.19	.33	.57	.42	.47
HM-rep		.94	.88	.90	.10	.99	.93	.96	.15	.81	.58	.68	.13	.96	.69	.80	.24	.64	.39	.48	.15	.89	.55	.67	.33
RG-rep		.91	.87	.89	.10	.98	.94	.96	.17	.62	.55	.58	.17	.90	.80	.85	.33	.36	.40	.38	.17	.60	.66	.63	.40
HM-rep	Single-encoder	.91	.85	.88	.10	.99	.92	.95	.17	.77	.51	.61	.14	.97	.64	.77	.26	.61	.37	.46	.16	.87	.52	.65	.37
	Array-encoder	.93	.86	.89	.09	.99	.91	.95	.15	.78	.57	.66	.15	.97	.71	.82	.26	.61	.41	.49	.15	.85	.57	.68	.35
	Combined	.94	.88	.90	.10	.99	.93	.96	.15	.81	.58	.68	.13	.96	.69	.80	.24	.64	.39	.48	.15	.89	.55	.67	.33
HM-rep (10%*)	Single-encoder	.82	.60	.69	.14	.97	.71	.82	.24	.67	.37	.48	.16	.92	.51	.65	.32	.54	.27	.36	.17	.86	.42	.57	.39
	Array-encoder	.89	.68	.77	.12	.98	.74	.85	.19	.75	.51	.61	.16	.96	.66	.78	.28	.60	.36	.45	.15	.89	.53	.67	.36
	Combined	.89	.71	.79	.11	.98	.78	.87	.19	.73	.55	.63	.15	.94	.71	.80	.27	.56	.38	.45	.16	.82	.56	.67	.36

*model trained using 10% of training set

Pre → Precision; Rec → Recall

TABLE IV: Generalization towards the number of sources and musical genres (model trained with Combined architecture and HM-rep; metric calculated with 1 meter resolution)

(a) Number of Sources

Dataset	# of Srcs	Pre	Rec	F1↑	RMSE↓
test-S0	1	.99	.99	.99	.08
	2	.98	.89	.93	.18
test-S1	3	.96	.64	.77	.22
	1	.96	.81	.88	.22
test-A0	2	.96	.63	.76	.25
	3	.98	.46	.62	.27
test-R0	1	.90	.81	.85	.26
	2	.87	.39	.54	.40
test-R1	3	.87	.32	.46	.42

(b) Musical Genres

Dataset (genre)	Pre	Rec	F1↑	RMSE↓
test-S0 (c-f)	.99	.93	.96	.15
test-S2 (jazz)	.99	.95	.97	.13
test-A0 (c-f)	.96	.69	.80	.24
test-A2 (jazz)	.92	.54	.68	.37
test-R0 (c-f)	.89	.55	.67	.33
test-R2 (jazz)	.92	.54	.68	.39

Pre → Precision; Rec → Recall

from the real world with augmentation to the real world on *classical-funk* data. However it is not the case with *jazz* data. The reason is that *classical-funk* data contains lots of variations in loudness and silent pauses while *jazz* tends not to. In the real world with augmentation data, those weak intensity passages (where sources cannot be considered active) are filtered out whereas with real world data this is not possible.

V. CONCLUSION

This paper introduced a novel architecture as well as two novel output representations for deep learning based multiple sound source 2D localization. These lead to a significant improvement of the localization performance as shown by the extensive experiments conducted on both simulated and real-world data. A remaining issue is the performance degradation from the simulated environment to the real world. This is probably due to the insufficient amount of real world data for training a DNN. In the future, we plan to leverage simulation to inexpensively generate a large amount of labeled data and then train the localization model in such a way that the knowledge is transferable to the real world.

REFERENCES

- [1] S. Chakrabarty and E. A. Habets, "Multi-speaker localization using convolutional neural network trained with noise," in *Workshop Machine Learning for Audio Signal Processing at NIPS (MLAudio@NIPS17)*.
- [2] W. He, P. Motlicek, and J. Odobez, "Deep neural networks for multiple speaker detection and localization," in *2018 IEEE International Conference on Robotics and Automation (ICRA)*, May 2018, pp. 74–79.
- [3] W. He, P. Motlicek, and J.-M. Odobez, "Joint localization and classification of multiple sound sources using a multi-task neural network," in *Proc. Interspeech 2018*, 2018, pp. 312–316.
- [4] M. Cobos, F. Antonacci, A. Alexandridis, A. Mouchtaris, and B. Le, "A survey of sound source localization methods in wireless acoustic sensor networks," *Wireless Communications and Mobile Computing*, 2017.
- [5] Wing-Kin Ma, Ba-Ngu Vo, S. S. Singh, and A. Baddeley, "Tracking an unknown time-varying number of speakers using tdoa measurements: a random finite set approach," *IEEE Transactions on Signal Processing*, vol. 54, no. 9, pp. 3291–3304, Sep. 2006.
- [6] A. Alexandridis and A. Mouchtaris, "Multiple sound source location estimation in wireless acoustic sensor networks using doa estimates: The data-association problem," *IEEE/ACM Trans. Audio, Speech and Lang. Proc.*, vol. 26, no. 2, pp. 342–356, Feb. 2018.
- [7] A. Griffin, A. Alexandridis, D. Pavlidis, Y. Mastorakis, and A. Mouchtaris, "Localizing multiple audio sources in a wireless acoustic sensor network," *Signal Processing*, vol. 107, pp. 54 – 67, 2015.
- [8] H. Sundar, T. V. Sreenivas, and C. S. Seelamantula, "Tdoa-based multiple acoustic source localization without association ambiguity," *IEEE/ACM Transactions on Audio, Speech, and Language Processing*, vol. 26, no. 11, pp. 1976–1990, Nov 2018.
- [9] T. Inoue, P. Vinayavekhin, S. Wang, D. Wood, N. Greco, and R. Tachibana, "Domestic activities classification based on CNN using shuffling and mixing data augmentation," DCASE2018 Challenge, Tech. Rep., September 2018.
- [10] R. Takeda and K. Komatani, "Discriminative multiple sound source localization based on deep neural networks using independent location model," in *2016 IEEE Spoken Language Technology Workshop (SLT)*, Dec 2016, pp. 603–609.
- [11] J. Vera-Diaz, D. Pizarro, and J. Macias-Guarasa, "Towards end-to-end acoustic localization using deep learning: From audio signals to source position coordinates," *Sensors*, vol. 18, no. 10, p. 3418, Oct 2018.
- [12] F. Vesperini, P. Vecchiotti, E. Principi, S. Squartini, and F. Piazza, "A neural network based algorithm for speaker localization in a multi-room environment," in *2016 IEEE 26th International Workshop on Machine Learning for Signal Processing (MLSP)*, Sep. 2016, pp. 1–6.
- [13] S. Adavanne, A. Politis, J. Nikunen, and T. Virtanen, "Sound event localization and detection of overlapping sources using convolutional recurrent neural networks," *IEEE Journal of Selected Topics in Signal Processing*, vol. 13, no. 1, pp. 34–48, March 2019.
- [14] S. Adavanne, A. Politis, and T. Virtanen, "Direction of arrival estimation for multiple sound sources using convolutional recurrent neural network," in *2018 26th European Signal Processing Conference (EU-SIPCO)*, Sep. 2018, pp. 1462–1466.
- [15] J. Redmon, S. Divvala, R. Girshick, and A. Farhadi, "You only look once: Unified, real-time object detection," in *2016 IEEE Conference on Computer Vision and Pattern Recognition (CVPR)*, June 2016.
- [16] R. Scheibler, E. Bezzam, and I. Dokmanic, "Pyroomacoustics: A python package for audio room simulation and array processing algorithms," in *2018 IEEE International Conference on Acoustics, Speech, and Signal Processing, ICASSP 2018 - Proceedings*, 9 2018.
- [17] A. Alexandridis, A. Griffin, and A. Mouchtaris, "Multiple source location estimation on a dataset of real recordings in a wireless acoustic sensor network," in *2018 IEEE 20th International Workshop on Multimedia Signal Processing (MMSP)*, Aug 2018, pp. 1–6.